

# On the very high energy ( $> 25\text{GeV}$ ) pulsed emission in the Crab pulsar.

Machabeli George<sup>1</sup> and Osmanov Zaza<sup>2</sup>

*Georgian National Astrophysical Observatory, Chavchavadze State University, Kazbegi 2a, 0106, Tbilisi, Georgia*

## ABSTRACT

We have examined the recently detected very high energy (VHE) pulsed radiation from the Crab pulsar. According to the observational evidence, the observed emission ( $> 25\text{GeV}$ ) peaks at the same phase with the optical spectrum. Considering the cyclotron instability, we show that the pitch angle becomes non-vanishing leading to the efficient synchrotron mechanism near the light cylinder surface. The corresponding spectral index of the emission equals  $-1/2$ . By studying the inverse Compton scattering and the curvature radiation, it is argued that the aforementioned mechanisms do not contribute to the VHE radiation detected by MAGIC.

*Subject headings:* instabilities - plasmas - pulsars: individual (PSR B0531+21) - radiation mechanisms: non-thermal

## 1. Introduction

For studying the high energy radiation of pulsars, two major mechanisms are used: the synchrotron process (Pacini 1971; Shklovsky 1970) and the Inverse Compton Scattering (ICS) (Blandford et al. 1990). However, the problem of identification of a location, where the radiation comes from still is a matter of discussion. For solving this problem an approach of the so-called polar cap model was proposed (Sturrock 1971). According to this model, due to very strong electrostatic field, particles are uprooted from the star's surface layer and accelerate along the magnetic field lines (Ruderman & Sutherland 1975) inside a zone where the electric field is nonzero (gap). This process leads to relativistic energies of electrons, which in turn, create radiation. Unfortunately, the particle energy inventory accumulated within the gap is not enough to explain the observed high energy emission. For solving this problem, to enlarge somehow the gap zone, series of works have been invoked. Arons & Scharlemann (1979) have considered an effect of rectifying the curved magnetic

field lines and they have shown that this process leads to an increase of the gap size. Harding et al. (1981) have applied the method developed by Arons & Scharlemann (1979) for studying the high altitude emission from the pulsar slot gaps. A three-dimensional model of optical and  $\gamma$ -ray emission from the slot gap accelerator was examined and it has been predicted that the emission below  $200\text{MeV}$  must exhibit correlations in time and phase with the radio band. Somewhat different mechanism leading to the effect of the gap size increase was proposed by Usov & Shabad (1985) where the intermediate formation of positronium (electron-positron bound state) was studied. Generally speaking, the space-time close to neutron star's surface is slightly curved. Based on this fact, Muslimov & Tsygan (1992) have considered an effect of creation of an additional electric field due to the influence of the Kerr metric. All aforementioned mechanisms cannot provide a significant increase of the gap size to explain the observed high energy radiation from pulsars. To solve this problem, the so-called outer gap model has been proposed [see for example (Cheng et al. 1986a,b)]. According to this approach radiation is formed further out in the magnetosphere of pul-

<sup>1</sup>g.machabeli@astro-ge.org

<sup>2</sup>z.osmanov@astro-ge.org

sars and mechanisms responsible for emission are: the synchrotron, inverse Compton and curvature radiation processes respectively.

Recently, MAGIC Cherenkov telescope has detected from the Crab pulsar the VHE pulsed emission above  $25\text{GeV}$  (Aliu et al. 2008). The most peculiar feature of the observed radiation is coincidence of the high energy and optical signals (Aliu et al. 2008). This indicates that the polar cap models cannot be applied for explaining the MAGIC observational data. In (Machabeli & Osmanov 2009) we have examined the Crab pulsar's recently observed VHE pulsed emission data. It is worth noting that due to very small cooling timescales, particles rapidly transit to the ground Landau state completely killing the subsequent radiation. We have found that due to the cyclotron instability, the optical spectrum is generated, which in turn via the quasi-linear diffusion provokes the increase of the pitch angles, leading to the synchrotron process with the spectral index  $-1/2$ . It has been shown that the emission in the optical and high energy ( $> 25\text{GeV}$ ) bands originate from the well localized regions, leading to the observational fact that the signals peak with the same phases. As we have already noted, the analysis of the observational data indicates that the curvature radiation and the inverse Compton mechanism must be excluded from the possible emission mechanisms. Generally speaking, for very strong corotating magnetic fields, the particles a) move along curved trajectories and b) accelerate up to relativistic energies. Therefore, it is of great importance to understand why the curvature radiation and the ICS are not involved in the process of emission.

The paper is organized as follows. In Section 2 we consider the synchrotron, Inverse Compton and curvature radiation mechanisms, in Sect. 3 we present our results and in Sect. 4 we summarize them.

## 2. Main consideration

In this section we are going to consider three major emission mechanisms: the synchrotron process, the ICS and the curvature radiation respectively.

### 2.1. Synchrotron emission

As we have already mentioned, timescales of transit of particles to the ground Landau state is very small and electrons very soon start moving along the magnetic field lines without emission. Machabeli & Usov (1979) have found that the situation changes due to the cyclotron instability, leading to creation of nonzero pitch angles and the corresponding radiation process. The method developed in (Machabeli & Usov (1979)) was applied by us in (Machabeli & Osmanov 2009). We have shown that the quasi-linear diffusion excites the transverse and longitudinal-transverse waves:

$$\omega_t = kc(1 - \delta_1), \quad (1)$$

$$\omega_{lt} = k_{\parallel}c(1 - \delta_1 - \delta_2) \quad (2)$$

where  $k$  is the modulus of the wave vector,  $k_{\parallel}$  and  $k_{\perp}$  are the wave vector's longitudinal (parallel to the magnetic field) and transverse (perpendicular to the magnetic field) components respectively,  $c$  is the speed of light and

$$\delta_1 = \frac{\omega_p^2}{4\omega_B^2\gamma_p^3}, \quad \delta_2 = \frac{k_{\perp}^2 c^2}{16\omega_p^2\gamma_p}, \quad (3)$$

where,  $\omega_p \equiv \sqrt{4\pi n_p e^2/m}$  is the plasma frequency,  $\omega_B \equiv eB/mc$  is the cyclotron frequency,  $e$  and  $m$  are electron's charge and the rest mass respectively and  $n_p$  is the plasma density. According to a model developed by Machabeli & Osmanov (2009), we consider the plasma composed of two components: a) the plasma component with the Lorentz factor,  $\gamma_p$  and b) the beam component with the Lorentz factor,  $\gamma_b$ .

Kazbegi et al. (1992) have shown that the aforementioned modes generate if the cyclotron resonance regime

$$\omega - k_{\parallel}V_{\parallel} - k_x u_x \pm \frac{\omega_B}{\gamma_b} = 0, \quad (4)$$

takes place.  $u_x \equiv cV_{\parallel}\gamma_b/\rho\omega_B$  is the drift velocity,  $V_{\parallel}$  is the longitudinal velocity component and  $\rho$  is the curvature radius of field lines.

For the parameters of the Crab pulsar,  $P \approx 0.033\text{sec}$ ,  $R_s \approx 10^6\text{cm}$ ,  $n_{ps} \approx 1.4 \times 10^{19}\text{cm}^{-3}$ ,  $B_s \approx 7 \times 10^{12}\text{G}$ ,  $\gamma_b \approx 10^8$ , from Eqs. (1-4) one can show that the development of the cyclotron instability occurs in the optical band ( $\sim 10^{15}$ ) close

to the light cylinder zone.  $P$  denotes the pulsar's period,  $R_s$  - its radius, and  $n_{ps}$  and  $B_s$  are the plasma density and the magnetic field induction respectively, close to the star.

When electrons emit in the synchrotron regime, they experience the so-called radiative forces (Landau & Lifshitz 1971):

$$F_{\perp} = -\alpha\psi(1 + \gamma_b^2\psi^2),$$

$$F_{\parallel} = -\alpha\gamma_b^2\psi^2, \quad \alpha = \frac{2}{3} \frac{e^2\omega_B^2}{c^2}, \quad (5)$$

where  $\psi$  is the pitch angle. These forces try to decrease the pitch angle contrary to the quasi-linear diffusion, which tends to widen the value of  $\psi$ . The dynamical process saturates when these two processes balance each other. As it has been shown (Machabeli & Osmanov 2009; Malov & Machabeli 2001), when  $\gamma\psi \gg 1$  the kinetic equation in the quasi-stationary regime ( $\partial/\partial t = 0$ ) reduces to

$$\frac{\partial [F_{\parallel}f]}{\partial p_{\parallel}} + \frac{1}{p_{\parallel}\psi} \frac{\partial [\psi F_{\perp}f]}{\partial \psi} = \frac{1}{\psi} \frac{\partial^2}{\partial \psi \partial p_{\parallel}} \left( D_{\perp\parallel} \frac{\partial f}{\partial \psi} \right) +$$

$$+ \frac{1}{\psi} \frac{\partial}{\partial \psi} \left[ \psi \left( D_{\perp\perp} \frac{\partial}{\partial \psi} + D_{\perp\parallel} \frac{\partial}{\partial p_{\parallel}} \right) f \right], \quad (6)$$

where  $f = f(\psi, p_{\parallel})$  is the distribution function of particles,  $p_{\parallel}$  is the longitudinal momentum,

$$D_{\perp\perp} \approx -\frac{\pi^2 e^2 n_b c}{2\omega}, \quad D_{\perp\parallel} \approx \frac{\pi^2 e^2 n_b \omega_B}{2mc\gamma^2 \omega^2}, \quad (7)$$

are the diffusion coefficients and  $n_b = B/(Pce)$  is the density of the beam component. This equation can be solved easily if one expresses the distribution function as  $\chi(\psi)f(p_{\parallel})$ . Then, after substituting this expression into Eq. (6) one gets following (Machabeli & Osmanov 2009; Chkheidze & Machabeli 2007):

$$\chi(\psi) = C_1 e^{-A\psi^4}, \quad f(p_{\parallel}) = \frac{C_2}{\left( \alpha \bar{\psi}^2 \gamma_b^2 - \frac{\pi^2 e^2 \bar{\psi} n_b c}{\gamma_b} \right)}, \quad (8)$$

where

$$A \equiv \frac{4e^6 B^4 P^3 \gamma_p^4}{3\pi^3 m^5 c^7 \gamma_b}, \quad (9)$$

and

$$\bar{\psi} = \frac{\int_0^\infty \psi \chi(\psi) d\psi}{\int_0^\infty \chi(\psi) d\psi} \approx \frac{0.5}{\sqrt[4]{A}}. \quad (10)$$

is the mean value of the pitch angle.

Relativistic electrons moving in the magnetic field emit photons with energies expressed by  $\epsilon \approx 1.2 \times 10^{-17} B \gamma^2 \sin \psi$  (e.g. Rybicki & Lightman 1979), which after applying Eq. (10) reduces to:

$$\epsilon_{syn}(GeV) \approx 6 \times 10^{-18} \left( \frac{3\pi^3 m^5 c^7 \gamma_b^9}{4P^3 e^6 \gamma_p^4} \right)^{\frac{1}{4}}. \quad (11)$$

According to the results of the MAGIC Cherenkov telescope (Aliu et al. 2008), the VHE ( $> 25 GeV$ ) pulsed radiation from the Crab pulsar peaks with the same phase as the optical signal. This circumstance is in a good agreement with our model, since, as we have shown, the pitch angles increase due to the cyclotron instability, which in its turn occurs in the optical frequency ranges.

Let us apply Eqs. (10,11) to the Crab pulsar. Then by taking into account the following parameters,  $R_s \approx 10^6 cm$ ,  $B_s \approx 7 \times 10^{12} G$  and  $\gamma_p \approx 3$ , one can show that the pitch angle is of the order of  $10^{-5}$ , which guarantees the observed high energy emission if  $\gamma_b \approx 3.2 \times 10^8$ . For the mentioned set of parameters one has  $\alpha \bar{\psi}^2 \gamma_b^2 \gg \pi^2 e^2 \bar{\psi} n_b c / \gamma_b$ , which reduces the distribution function to  $f(p_{\parallel}) \propto \gamma_b^{-2}$ . On the other hand, the spectrum of the synchrotron radiation behaves as  $I_\nu \propto \nu^{-\frac{\beta-1}{2}}$  (Ginzburg 1981), where  $\beta$  describes the particle distribution function,  $f \propto \gamma^{-\beta}$ . This indicates that, for the case considered in the present paper ( $\beta = 2$ ) the spectral index of the VHE synchrotron emission equals  $-1/2$ .

Therefore, as we see, the synchrotron emission can explain the observed VHE radiation, and as we have already seen, for this purpose the particles must have very high Lorentz factors. On the other hand, these particles will inevitably encounter soft photons, which in turn can also create the high energy radiation via the ICS. But in this case the emission will not be localized contrary to the observational evidence, indicating that for some reason the ICS is not involved in the process of the detected emission. The next subsection is dedicated to this particular problem.

## 2.2. Compton scattering

It is well known that when a photon with energy  $\epsilon$  encounters a relativistic electron, under certain conditions photons might gain energy. The cor-

responding frequency after scattering is given by (e.g. Rybicki & Lightman 1979):

$$\omega' = \omega \frac{1 - \beta \cos \theta}{1 - \beta \cos \theta' + \frac{\hbar \omega}{\gamma m c^2} (1 - \cos \theta'')}, \quad (12)$$

where  $\omega$  is the frequency before scattering,  $\beta \equiv v/c$ ,  $\theta = (\widehat{\mathbf{P}\mathbf{K}})$ ,  $\theta' = (\widehat{\mathbf{P}\mathbf{K}'})$ ,  $\theta'' = (\widehat{\mathbf{K}\mathbf{K}'})$ . By  $\mathbf{K}$  and  $\mathbf{K}'$  we denote the three momentum of the photon before and after scattering respectively. The momentum of relativistic electrons before scattering is denoted by  $\mathbf{P}$ .

Since, according to the observational evidence, we observe the well localized pulses of high energy emission, therefore the angle,  $\theta$  must be very small. On the other hand, analyzing the excitation of oblique waves in a relativistic electron-positron plasma one can argue that the pitch angle has to be extremely low (Volokitin et al. 1985). Then, Eq. (12) reduces to

$$\omega' \approx \omega \frac{1 - \beta}{1 - \beta \cos \theta' + \frac{\hbar \omega}{\gamma m c^2} (1 - \cos \theta'')}. \quad (13)$$

We will study two principally different cases: (a)  $\cos \theta' \ll 1$  and (b)  $\cos \theta' \sim 1$ . In the first case, we have

$$\omega' \approx \frac{\omega}{2\gamma^2} \times \frac{1}{1 + \frac{\hbar \omega}{\gamma m c^2} (1 - \cos \theta'')}, \quad (14)$$

where we have taken into account the following approximate relation,  $1 - \beta \approx 1/2\gamma^2$  for  $\beta \sim 1$ . From this expression we see that for all physical quantities the frequency after the scattering is less than that of before the scattering and therefore, there is no possibility of increasing  $\omega$  to the VHE band.

By considering the second limit, Eq. (13) reduces to

$$\omega' \approx \omega \frac{1}{1 + \frac{2\hbar \omega \gamma}{m c^2} (1 - \cos \theta'')}, \quad (15)$$

which, as in the previous case, leads to the similar result,  $\omega' < \omega$ .

This investigation shows that the ICS cannot provide the VHE radiation from the Crab pulsar detected by MAGIC (Aliu et al. 2008).

### 2.3. Curvature radiation

Since particles are moving along the curved magnetic field lines continuously, they will emit

the curvature radiation. On the other hand, in Eq. (6) we have neglected a term corresponding to the curvature emission. This in its turn, means that the following ratio

$$\eta \equiv \frac{\epsilon_{cur}}{\epsilon_{syn}}, \quad (16)$$

where (Ruderman & Sutherland 1975)

$$\epsilon_{cur} = \frac{3\hbar}{2} \gamma_b^3 \times \frac{c}{\rho}, \quad (17)$$

and  $\rho$  is the curvature radius of magnetic field lines, must be less than one. By applying Eqs. (11,16,17), one can show that for typical magnetospheric parameters of the Crab pulsar close to the light cylinder, the aforementioned ratio is negligible only if the curvature radius exceeds the light cylinder radius,  $R_{lc}$ , approximately by three orders of magnitude.

Generally speaking, since no contribution in emission comes from the closed magnetic field lines, we consider the open ones. On the other hand, in the dipolar field the region of almost straight field lines is just a tiny fraction of the emission area, leading to a negligible value of the high energy luminosity.

If the beam component particles move along curved field lines, they experience the so-called curvature drift with the velocity:

$$u_b = \frac{\gamma_b v_{\parallel}^2}{\omega_{B_b} \rho}, \quad (18)$$

where  $\omega_{B_b} = eB_0/mc$ ; and  $B_0$  is the background magnetic field induction. This velocity will eventually create the drift current,  $J_{dr} = en_b u_b$  which in turn, via the Maxwell equation

$$(\nabla \times \mathbf{B})_x = \frac{4\pi}{c} J_{dr}, \quad (19)$$

can create the toroidal magnetic field (by  $x$  we denote a direction of the drift current. See Fig. 1). This current is evidently less than the Goldreich-Julian (GJ) current  $J_{GJ} = en_b c$ , since  $u_b \ll c$ . But on the other hand, the GJ current creates the corresponding magnetic field,  $B_r \approx 4\pi J_{GJ} R_n / c$ , where  $R_n \approx B(R)/B'(R) = R/3$  ( $B' \equiv dB/dR$ ) is the length scale of the spatial inhomogeneity of the magnetic field. If we assume a dipolar configuration, then, by taking the value of the GJ density,

$n_b \approx \Omega B / (2\pi e c)$ , into account, one can show that the toroidal magnetic field equals  $\frac{2R}{3R_c} B$ . Inside the light cylinder ( $R < R_c$ ), this value is less than the background magnetic field- $B$  and therefore such a toroidal magnetic field will be unable to rectify the twisted magnetic field lines. This implies that the curvature drift current, which is less than that of the GJ, cannot contribute to the process of rectifying the field lines. However, in spite of that the drift current is not the source of the toroidal component,  $B_r$ , it is a trigger mechanism for generation the perturbed current,  $J_1 = e(n_b^0 v_{bx}^1 + n_b^1 u_b)$  responsible for the creation of  $B_r$  (see Eq. (A10)), where by upper script "1" we denote the perturbed quantities. The source of the instability of current and the resulting magnetic field is the pulsar's rotational energy and the process is achieved via the parametrically excited curvature drift waves. The corresponding increment of the curvature drift instability can be presented by (see Appendix, for more details see (Osmanov et al. 2008, 2009)):

$$\Gamma \approx \left( -\frac{3}{2} \frac{\omega_b^2}{\gamma_{b0}} \frac{k_x u_b}{k_\theta c} \right)^{1/2} \left| J_0 \left( \frac{k_x u_b}{4\Omega} \right) J_0 \left( \frac{k_\theta c}{\Omega} \right) \right|, \quad (20)$$

where  $\omega_b$  is the beam component plasma frequency and  $\gamma_{b0}$  - the Lorentz factor in an unperturbed state.  $k_x$  and  $k_\theta$  are the wave vector's components and  $\Omega$  is the angular velocity of rotation.

By considering the typical magnetospheric parameters for the Crab pulsar close to the light cylinder,  $P \approx 0.033s$ ,  $\gamma_{b0} = 10^8$  and examining the perturbation lengthscale  $\lambda \approx 10^8 cm$  (Osmanov et al. 2009), one can see that the increment is of the order of  $1s^{-1}$ . Comparing this value with the Crab pulsar's slowdown rate,  $4.2 \times 10^{-13}s^{-1}$ , we see that the instability growth rate exceeds by many orders of magnitude the slowdown rate, indicating that the mentioned instability is extremely efficient.

It is worth noting that we have three types of the open field lines: (a) curved field lines which pass ahead of the rotation; (b) a tiny fraction of almost straight field lines and (c) curved field lines, lagging behind the rotation.

If the initial perturbation of the toroidal magnetic field satisfies the condition  $B_r > 0$ , then such a perturbation will rectify all field lines which initially pass ahead of the rotation (suppose the clockwise rotation of the system) and will twist

even more the magnetic field lines, which initially lag behind the rotation. In the case,  $B_r < 0$ , the situation is opposite: the field lines initially lagging behind the rotation will be rectified. At this stage the curvature becomes infinity and as we see from Eq. (18), the drift velocity tends to zero, saturating (killing) the instability.

The investigation shows that, the curvature drift instability provides necessary conditions for an efficient mechanism of rectifying the field lines, leading to the negligible role of the curvature radiation, confirming our assumptions leading to Eq. (6).

### 3. Summary

1. We have considered several emission mechanisms for explaining the recently detected VHE emission from the Crab pulsar.
2. Studying the synchrotron mechanism, we have shown that due to the cyclotron instability efficiently developing on light cylinder scales, non-vanishing pitch angles are created, that leads to the efficient high energy synchrotron emission with the spectral index  $-1/2$ .
3. The observational fact of the coincidence of signals in optical and high energy ( $> 25GeV$ ) intervals is in a good agreement with our model, in the framework of which, the cyclotron instability is excited in the optical spectra, which, via the synchrotron process leads to the high energy emission.
4. Analyzing the inverse Compton scattering, we have found that for Crab pulsar's magnetospheric parameters even very energetic electrons are unable to produce the observed photon energies.
5. Considering the curvature radiation, we show that due to the curvature drift instability, the magnetic field lines are rectified very efficiently. This in turn, leads to a negligible role of the curvature emission process in the observed VHE emission along the aforementioned rectified field lines.

As we see, the detected coincidence of VHE and optical signals is an indirect confirmation of

the fact that (a) both spectra is produced by one source and (b) the only mechanism providing the detected high energy radiation is the synchrotron mechanism. This means that we observe the Crab pulsar towards these straight field lines, that is the reason why we do not see the curvature radiation coming from the twisted magnetic field lines.

### **Acknowledgments**

The research was supported by the Georgian National Science Foundation grant GNSF/ST06/4-096.

### A. Curvature drift instability

In this section we study the process of rectifying the magnetic field lines due to the parametrically excited curvature drift instability. This instability is called parametric, because an external force - centrifugal force, plays a role of a parameter, changes in time and creates the instability. Generally speaking, the presence of an external varying parameter generates the plasma instability. The mechanism of energy pumping process from the external alternating electric field into the electron-ion plasma is quite well investigated in (Silin 1973; Galeev & Sagdeev 1973; Max 1973). Instead of considering the altering electric field, one can examine the centrifugal force as a varying parameter (Machabeli et al. 2005).

We start our consideration by supposing that the magnetic field lines are almost straight with very small nonzero curvature (see Fig. 1). In this context we examine the field lines that are open, and thus have the curvature radius exceeding the light cylinder one, maximum by one order. Therefore, dynamics of particles, governing the overall picture of the curvature drift instability, can be studied, assuming that field lines are almost straight. In the framework of the paper we suppose that the plasma flow consists of two components: the plasma component composed of electrons and positrons ( $e^\pm$ ); and, the so-called, beam component ( $b$ ) composed of relativistic electrons. It is well known that the dynamics of plasma particles moving along the straight co-rotating magnetic field lines is described by the Euler equation: (Machabeli et al. 2005):

$$\frac{\partial \mathbf{p}_\alpha}{\partial t} + (\mathbf{v}_\alpha \nabla) \mathbf{p}_\alpha = -c^2 \gamma_\alpha \xi \nabla \xi + \frac{e_\alpha}{m} \left( \mathbf{E} + \frac{1}{c} \mathbf{v}_\alpha \times \mathbf{B} \right), \quad (\text{A1})$$

where  $\xi \equiv \sqrt{1 - \Omega^2 R^2 / c^2}$ ,  $R$  is the coordinate along the straight field lines;  $\mathbf{p}_\alpha$ ,  $\mathbf{v}_\alpha$ , and  $e_\alpha$  are the momentum (normalized to the particle's mass), the velocity and the charge of electrons/positrons, respectively;  $\alpha = \{e^\pm, b\}$  denotes the sort of particles and  $\mathbf{E}$  and  $\mathbf{B}$  are the electric and the magnetic field induction respectively. The continuity equation:

$$\frac{\partial n_\alpha}{\partial t} + \nabla(n_\alpha \mathbf{v}_\alpha) = 0, \quad (\text{A2})$$

and the induction equation:

$$\nabla \times \mathbf{B} = \frac{1}{c} \frac{\partial \mathbf{E}}{\partial t} + \frac{4\pi}{c} \sum_{\alpha=e^\pm, b} \mathbf{J}_\alpha, \quad (\text{A3})$$

(where  $n_\alpha$  and  $\mathbf{J}_\alpha$  are the density and the current, respectively) complete the set of equations for  $n$ ,  $\mathbf{v}$ ,  $\mathbf{E}$  and  $\mathbf{B}$ .

In the leading state the plasma is in the frozen-in condition:  $\mathbf{E}_0 + \frac{1}{c} \mathbf{v}_{0\alpha} \times \mathbf{B}_0 = 0$ , then, one can show that the solution to the Euler equation in Eq. (A1) for ultra relativistic particle velocities in the leading state is given by (Machabeli & Rogava 1994):

$$v_\theta^0 \equiv v_\parallel = c \cos(\Omega t + \varphi), \quad (\text{A4})$$

where  $v_\parallel$  is the velocity component along the magnetic field lines and  $\varphi$  is the initial phase of each particle.

For solving the set of Eqs. (A1-A3), we will linearize it assuming that, in the zeroth order of approximation, the flow has the longitudinal velocity satisfying Eq. (A4) and also drifts along the  $x$ -axis driven by the curvature of magnetic field lines (see Fig. 1):

$$u_\alpha = \frac{\gamma_{\alpha 0} v_\parallel^2}{\omega_{B_\alpha} \rho}, \quad (\text{A5})$$

where  $u_\alpha$  is the drift velocity;  $\omega_{B_\alpha} = e_\alpha B_0 / mc$ ; and  $B_0$  is the background magnetic induction.

Let us expand the physical quantities up to the first order terms:

$$\Psi \approx \Psi^0 + \Psi^1, \quad (\text{A6})$$

where  $\Psi \equiv \{n, \mathbf{v}, \mathbf{p}, \mathbf{E}, \mathbf{B}\}$ . Then if we examine only the  $x$  components of Eqs. (A1,A3), and express the perturbed quantities as follows:

$$\Psi^1(t, \mathbf{r}) \propto \Psi^1(t) \exp[i(\mathbf{k}\mathbf{r})], \quad (\text{A7})$$

by taking into account that  $k_\theta \ll k_x$  and  $k_r = 0$ , and bearing in mind that  $v_r^1 \approx cE_x^1/B_0$ , one can show that Eqs. (A1-A3) reduce to the form:

$$\frac{\partial p_{\alpha x}^1}{\partial t} - i(k_x u_\alpha + k_\theta v_\parallel) p_{\alpha x}^1 = \frac{e_\alpha}{mc} v_\parallel B_r^1, \quad (\text{A8})$$

$$\frac{\partial n_\alpha^1}{\partial t} - i(k_x u_\alpha + k_\theta v_\parallel) n_\alpha^1 = i k_x n_\alpha^0 v_{\alpha x}^1, \quad (\text{A9})$$

$$-i k_\theta c B_r^1 = 4\pi \sum_{\alpha=e^\pm, b} e_\alpha (n_\alpha^0 v_{\alpha x}^1 + n_\alpha^1 u_\alpha). \quad (\text{A10})$$

According to the standard method (Osmanov et al. 2008), after expressing  $v_{\alpha x}^1$  and  $n_\alpha^1$  in the following way:

$$v_{\alpha x}^1 \equiv V_{\alpha x} e^{i\mathbf{k}\mathbf{A}_\alpha(t)}, \quad (\text{A11})$$

$$n_\alpha^1 \equiv N_\alpha e^{i\mathbf{k}\mathbf{A}_\alpha(t)}, \quad (\text{A12})$$

$$A_{\alpha x}(t) = \frac{u_\alpha}{2\Omega} (\Omega t + \varphi) + \frac{u_\alpha}{4\Omega} \sin[2(\Omega t + \varphi)], \quad (\text{A13})$$

$$A_{\alpha \theta}(t) = \frac{c}{\Omega} \sin(\Omega t + \varphi), \quad (\text{A14})$$

and substituting them into Eqs. (A8,A9), one can get the expressions:

$$v_{\alpha x}^1 = \frac{e_\alpha}{mc\gamma_{\alpha 0}} e^{i\mathbf{k}\mathbf{A}_\alpha(t)} \int^t e^{-i\mathbf{k}\mathbf{A}_\alpha(t')} v_\parallel(t') B_r(t') dt', \quad (\text{A15})$$

$$n_\alpha^1 = \frac{i e_\alpha n_\alpha^0 k_x}{mc\gamma_{\alpha 0}} e^{i\mathbf{k}\mathbf{A}_\alpha(t)} \int^t dt' \int^{t''} e^{-i\mathbf{k}\mathbf{A}_\alpha(t'')} v_\parallel(t'') B_r(t'') dt'', \quad (\text{A16})$$

which combined with Eq. (A10), lead to the following form:

$$\begin{aligned} -i k_\theta c B_r^1(t) &= \sum_{\alpha=e^\pm, b} \frac{\omega_\alpha^2}{\gamma_{\alpha 0} c} e^{i\mathbf{k}\mathbf{A}_\alpha(t)} \int^t e^{-i\mathbf{k}\mathbf{A}_\alpha(t')} v_\parallel(t') B_r(t') dt' + \\ &+ i \sum_{\alpha=e^\pm, b} \frac{\omega_\alpha^2}{\gamma_{\alpha 0} c} k_x u_\alpha e^{i\mathbf{k}\mathbf{A}_\alpha(t)} \int^t dt' \int^{t''} e^{-i\mathbf{k}\mathbf{A}_\alpha(t'')} v_\parallel(t'') B_r(t'') dt'', \end{aligned} \quad (\text{A17})$$

where  $\omega_\alpha = e\sqrt{4\pi n_\alpha^0/m}$  represents the plasma frequency. If we apply the following identity:

$$e^{\pm i x \sin y} = \sum_s J_s(x) e^{\pm i s y}, \quad (\text{A18})$$

to Eq. (A17), the latter will simplify to the following form:

$$B_r(\omega) = - \sum_{\alpha=e^\pm, b} \frac{\omega_\alpha^2}{2\gamma_{\alpha 0} k_\theta c} \sum_{\sigma=\pm 1} \sum_{s, n, l, p} \frac{J_s(g_\alpha) J_n(h) J_l(g_\alpha) J_p(h)}{\omega + \frac{k_x u_\alpha}{2} + \Omega(2s + n)} \times$$



$$\begin{aligned}
& \times B_r(\omega + \Omega(2[s-l] + n - p + \sigma)) \left[ 1 - \frac{k_x u_\alpha}{\omega + \frac{k_x u_\alpha}{2} + \Omega(2s + n)} \right] \times \\
& \quad \times e^{i\varphi(2[s-l] + n - p + \sigma)} + \\
& + \sum_{\alpha=e^\pm, b} \frac{\omega_\alpha^2 k_x u_\alpha}{4\gamma_{\alpha 0} k_\theta c} \sum_{\sigma, \mu=\pm 1} \sum_{s, n, l, p} \frac{J_s(g_\alpha) J_n(h) J_l(g_\alpha) J_p(h)}{\left(\omega + \frac{k_x u_\alpha}{2} + \Omega(2[s+\mu] + n)\right)^2} \times \\
& \quad \times B_r(\omega + \Omega(2[s-l+\mu] + n - p + \sigma)) \times e^{i\varphi(2[s-l+\mu] + n - p + \sigma)}, \tag{A19}
\end{aligned}$$

where

$$g_\alpha = \frac{k_x u_\alpha}{4\Omega}, \quad h = \frac{k_\theta c}{\Omega}$$

and  $J_s(x)$  ( $s = 0; \pm 1; \pm 2 \dots$ ) is the Bessel function of integer order (Abramovitz & Stegan 1965).

In order to solve Eq. (A19), one has to examine similar equations, rewriting Eq. (A19) (with shifted arguments) for  $B_r(\omega \pm \Omega)$ ,  $B_r(\omega \pm 2\Omega)$ , etc.. This implies that we have to solve the system with the infinite number of equations, making the problem impossible to handle. Therefore, the only way is to consider the physics close to the resonance condition, that provides the cutoff of the infinite row in Eq. (A19) and makes the problem solvable (Silin & Tikhonchuk 1970).

Studying the resonance condition of Eq. (A19), one can derive the proper frequency for the CDI:

$$\omega_0 \approx -\frac{k_x u_\alpha}{2}. \tag{A20}$$

The present condition for physically meaningful case  $k_x u_\alpha/2 < 0$  implies that  $2s + n = 0$  and  $2[s+\mu] + n = 0$ .

For solving Eq. (A19), we examine the average value of  $B_r$  with respect to  $\varphi$ . Then, by taking into account the formula:

$$\frac{1}{2\pi} \int e^{iN\varphi} d\varphi = \delta_{N,0},$$

and preserving only the leading terms of Eq. (A19), after neglecting the contribution from the plasma components, one can derive the dispersion relation for the instability (Osmanov et al. 2008):

$$\left(\omega + \frac{k_x u_b}{2}\right)^2 \approx \frac{3\omega_b^2 k_x u_b}{2\gamma_{b0} k_\theta c} \left[ J_0\left(\frac{k_x u_b}{4\Omega}\right) J_0\left(\frac{k_\theta c}{\Omega}\right) \right]^2. \tag{A21}$$

By expressing the frequency as  $\omega \equiv \omega_0 + i\Gamma$  it is easy to estimate the increment of the CDI:

$$\Gamma \approx \left( -\frac{3}{2} \frac{\omega_b^2}{\gamma_{b0}} \frac{k_x u_b}{k_\theta c} \right)^{1/2} \left| J_0\left(\frac{k_x u_b}{4\Omega}\right) J_0\left(\frac{k_\theta c}{\Omega}\right) \right|. \tag{A22}$$

## REFERENCES

- Abramovitz, M. & Stegun, I., 1965, Handbook of Mathematical Functions, (eds.: Dover Publications Inc.: New York), p. 320
- Aliu E. et al., 2008, ApJ, **674**, 1037A
- Arons J. & Scharleman E.T., 1979, ApJ, **231**, 854
- Blandford R.D., Netzer H. & Woltjer L., 1990, Active Galactic Nuclei, Springer-Verlag
- Cheng K.S., Ho C. & Ruderman M., 1986, ApJ, **300**, 500
- Cheng K.S., Ho C. & Ruderman M., 1986, ApJ, **300**, 522
- Chkheidze N. & Machabeli G., 2007, **471**, 599
- Galeev & Sagdeev, 1973, Nucl. Fusion, 13, 603
- Ginzburg V.L., 1981, "Teor. Fizika i Astrofizika", Nauka M. 1981
- Harding A.K., Stern J.V., Dyks J. & Frackowiak M., 2008, ApJ, **680**, 1378
- Kazbegi A.Z., Machabeli G.Z. & Melikidze G.I., 1992, in Proc. IAU Collog. 128, The Magnetospheric Structure and Emission Mechanisms of Radio Pulsars, ed. T.H. Hankins, J.M: Rankin & J.A: Gil (Zielona Gora: Pedagogical Univ. Press), 232
- Landau L.D. & Lifshitz E.M., 1971, Classical Theory of Fields (London: Pergamon)
- Machabeli G., Osmanov Z. & Mahajan S., 2005, Phys. Plasmas 12, 062901
- Machabeli G. & Osmanov Z., 2009, ApJ(accepted)
- Machabeli, G.Z. & Rogava, A. D., 1994, Phys.Rev. A, 50, 98
- Machabeli G.Z. & Usov V.V., 1979, AZhh Pis'ma, **5**, 445
- Malov I.F. & Machabeli G.Z., 2001, ApJ, 554, 587
- Muslimov A.G. & Tsygan A.I., 1992, MNRAS, **255**, 61
- Max C., 1973, Phys. Fluids, 16, 1480
- Osmanov, Z., Dalakishvili, Z. & Machabeli, Z. 2008, MNRAS, 383, 1007
- Osmanov, Z., Shapakidze, D. & Machabeli, Z. 2008, (accepted for publication)
- Pacini F., 1971, ApJ, 163, 117
- Rybicki G.B. & Lightman A. P., 1979, Radiative Processes in Astrophysics. Wiley, New York
- Ruderman M.A. & Sutherland P.G., 1975, ApJ, 196, 51
- Shklovsky I.S., 1970, ApJ, 159, L77
- Silin V.P. & Tikhonchuk V.T., 1970, J. Appl. Mech. Tech. Phys., 11, 922
- Silin V.P., 1973, 'Parametricheskoe Vozdeistvie izlucheniya bol'shoj moshnosti na plazmu', Nauka, Moskva
- Sturrock P.A., 1971, ApJ, **164**, 529
- Usov V.V., Shabad A., 1985, Ap&SS, **117**, 309
- Volokitin, A. S., Krasnosel'skikh, V. V., Machabeli, G. Z., 1985, Sov. J. Plasma Phys., 11, 310

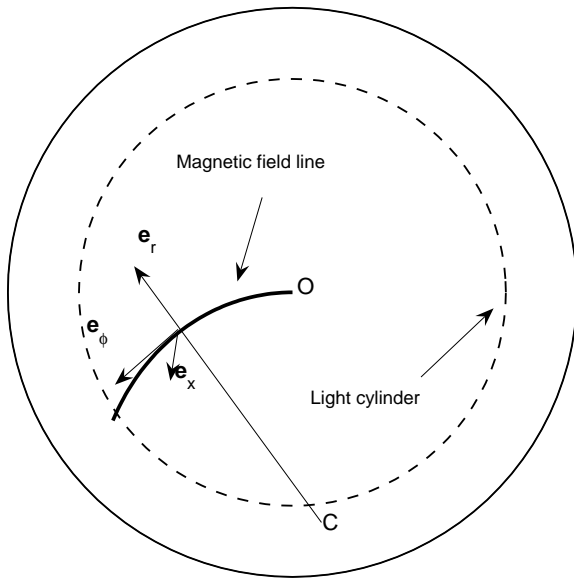


Fig. 1.— Here we show geometry in which we consider our system of equations. By  $\mathbf{e}_\phi$ ,  $\mathbf{e}_r$  and  $\mathbf{e}_x$  unit vectors are denoted, note that  $\mathbf{e}_x \perp \mathbf{e}_{r,\phi}$ .  $O$  is the center of rotation and  $C$  - the curvature center.